Chemical sensing with graphene: A quantum field theory perspective

Horacio Falomir,[1] Marcelo Loewe,[2,3,4] and Enrique Muñoz[2,5,*]

[1]*Facultad de Ciencias Exactas de la UNLP, IFLP, CONICET, Departamento de Física, C.C. 67, (1900) La Plata, Argentina*

[2]*Facultad de Física, Pontificia Universidad Católica de Chile, Vicuña Mackenna 4860, Santiago, Chile*

[3]*Centro Científico Tecnológico de Valparaíso, CCTVAL, Universidad Técnica Federico Santa María, Casilla 110-V, Valparaíso, Chile*

[4]*Centre for Theoretical and Mathematical Physics, University of Cape Town, Rondebosch 770, South Africa*

[5]*Center for Nanotechnology and Advanced Materials CIEN-UC, Avenida Vicuña Mackenna 4860, Santiago, Chile*

(Received 9 March 2021; revised 11 June 2021; accepted 14 June 2021; published 28 June 2021)

We studied theoretically the effect of a low concentration of adsorbed polar molecules on the optical conductivity of graphene, within the Kubo linear response approximation. Our analysis is based on a continuum model approximation that includes up to next-to-nearest neighbors in the pristine graphene effective Hamiltonian. Our results show that the conductivity can be expressed in terms of renormalized quasiparticle parameters $\tilde{v}_F$, $\tilde{M}$, and $\tilde{\mu}$ that include the effect of the molecular surface concentration $n_{\rm dip}$ and dipolar moment $\mathcal{P}$, thus providing a quantum field theory approach to model a graphene-based chemical sensor.

DOI: 10.1103/PhysRevB.103.235431

I. INTRODUCTION

The remarkable transport properties of graphene [1–5], as well as its affinity for the physisorption of different molecules, has attracted much attention toward its application as a field-effect transistor (FET) in chemical sensing [6–9]. In particular, the detection of polar molecules in gas phase has been investigated both experimentally as well as theoretically [9–12], with the later approach mainly based on *ab initio* methods. While providing an accurate prediction of the electronic structure for single adsorbed molecules [13], *ab initio* methods are not suitable to describe molecular concentrations, finite temperature, and disorder effects. On the other hand, as a complement with those numerical studies, the effects of molecular concentration, disorder, and finite temperature can be described by analytical models based on the continuum Dirac approximation within quantum field theory [14–17], thus providing an intuitive and accurate [18] picture of the underlying physical phenomena. Moreover, with appropriate approximations, these analytical models can often provide explicit formulas that are useful to interpret actual experiments. In this work, we present a quantum field theory that describes the optical conductivity in graphene under a given concentration of adsorbed polar molecules. This theory is a direct application of our previous work [17,19], based on a continuum description of graphene involving the effects of up to next-to-nearest neighbors on the underlying atomistic tight-binding Hamiltonian [20], which is analyzed by means of quantum field theory methods to include the electrostatic effects of adsorbed polar molecules on the surface of graphene. In the present model, we assume that the spatial distribution, as well as the orientation of the dipole moments of the adsorbed molecules, is disordered, and hence we obtain a quantum field theory representation for the optical conductance by performing a statistical average over these effects. The continuum model describing pristine graphene is summarized by the Lagrangian density [17,19]

$$\mathcal{L} = \frac{i}{2}[\psi^\dagger \partial_t \psi - \partial_t \psi^\dagger \psi] + \psi^\dagger e A_0 \psi - \frac{1}{2M}\{[(\mathbf{p} - e\mathbf{A} + \theta\boldsymbol{\sigma})\psi]^\dagger \cdot [(\mathbf{p} - e\mathbf{A} + \theta\boldsymbol{\sigma})\psi] - 2\theta^2 \psi^\dagger \psi\}, \quad (1)$$

with $\theta = M v_F$, and the effective-mass parameter [17,19,20] $M = -2/(9t' a_0^2) < 0$ capturing the effect of next-to-nearest-neighbor hopping t' on the continuum energy spectrum near both Dirac points.

II. SCATTERING BY RANDOMLY ADSORBED MOLECULES

We assume for simplicity that the electric properties of a single molecule adsorbed at a distance $a > 0$ above the surface of graphene can be modeled through a dipole potential, with two point charges $+Q$ and $-Q$ located at $(\mathbf{d}/2, a)$ and $(-\mathbf{d}/2, a)$, respectively, with $\mathbf{d}$ a two-dimensional (2D) vector. The corresponding potential at a position $\mathbf{r} = (x, y, 0)$ on the surface of graphene ($z = 0$) is

$$V_{\mathbf{d}}(\mathbf{r}) = \frac{\mathcal{P}}{4\pi\epsilon d}\left(\frac{1}{\sqrt{(\mathbf{r}-\mathbf{d}/2)^2 + a^2}} - \frac{1}{\sqrt{(\mathbf{r}+\mathbf{d}/2)^2 + a^2}}\right), \quad (2)$$

*munozt@fis.puc.cl

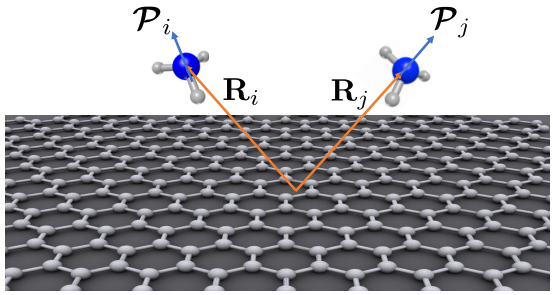

FIG. 1. Pictorial (not in actual scale) representation of polar molecules adsorbed at positions $\mathbf{R}_i$ and $\mathbf{R}_j$ on the surface of graphene.

with $\mathcal{P} = Q\mathbf{d}$ the dipole moment of the molecule and ϵ the local dielectric permittivity. The strict dipole approximation corresponds to the limit $d \to 0$, while $\mathcal{P}$ remains finite. In this limit, the 2D Fourier transform of the potential in Eq. (2) reduces to (see Appendix A)

$$\hat{V}_{\mathcal{P}}(\mathbf{q}) = \lim_{d\to 0} \hat{V}_{\mathbf{d}}(\mathbf{q}) = \frac{i\mathcal{P}\cdot\mathbf{q}}{2\epsilon q} e^{-qa}. \tag{3}$$

Let us now consider the effect of scattering by adsorbed polar molecules, randomly distributed with a surface concentration n_{dip}, on the optical conductivity of graphene (see Fig. 1). For this purpose, we first analyze their effect on the effective propagators arising from the Lagrangian Eq. (1) at finite temperature. A given realization within the ensemble of adsorbed molecular configurations is given by the potential

$$V(\mathbf{r}) = \sum_{j=1}^{N} V_{d_j}(\mathbf{r} - \mathbf{R}_j). \tag{4}$$

The basic assumptions are that the positions $\mathbf{R}_j$, as well as the orientations of the dipolar moments $\mathcal{P}_j$, are independent and identically distributed random variables, i.e.,

$$\langle \mathbf{R}_i \cdot \mathbf{R}_j \rangle = \delta_{ij} \langle \mathbf{R}^2 \rangle, \quad \langle \mathcal{P}_i \cdot \mathcal{P}_j \rangle = \delta_{ij} \frac{\mathcal{P}^2}{2}, \tag{5}$$

where in the last equation we further assumed that the dipole orientations are uniformly distributed in the azimuthal angle. Using standard diagrammatic methods and an average over disorder [21], it is shown (see Appendix A for details) that for low molecular concentrations n_{dip}, the scattering effects are correctly described by a disorder-averaged self-energy of the form (see Appendix A)

$$\hat{\Sigma}(i\omega_n, \mathbf{p}) = n_{\text{dip}} \int \frac{d^2q}{(2\pi)^2} |\hat{V}_{\text{avg}}(\mathbf{p}-\mathbf{q})|^2 \hat{\Delta}_E(i\omega_n, \mathbf{q}). \tag{6}$$

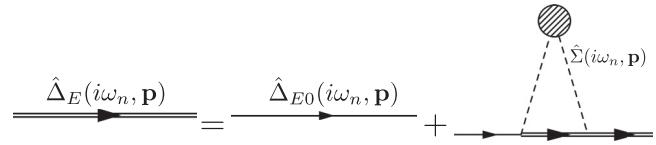

FIG. 2. The Feynman diagram corresponding to the Dyson equation for the dressed propagator. The self-energy is expressed by Eq. (6).

Here, $\omega_n = (2n+1)\pi T$ for $n \in \mathbb{Z}$ are fermionic Matsubara frequencies in the finite-temperature (Euclidean) representation, while $\hat{\Delta}_E(i\omega_n, \mathbf{p})$ is the fully dressed propagator arising from the solution of the Dyson equation (as depicted in Fig. 2)

$$\hat{\Delta}_E^{-1}(i\omega_n, \mathbf{p}) = \hat{\Delta}_{E0}^{-1}(i\omega_n, \mathbf{p}) - \hat{\Sigma}(i\omega_n, \mathbf{p}). \tag{7}$$

The Fourier transform of the dipole potential, averaged over dipole orientations, is defined as (see Appendix A)

$$|\hat{V}_{\text{avg}}(\mathbf{p})|^2 = \frac{1}{2}\frac{e^2\mathcal{P}^2}{4\epsilon^2} e^{-2pa}. \tag{8}$$

From our previous work [17,19], the bare, finite-temperature inverse (Euclidean) propagator is given by the expression

$$\hat{\Delta}_{E0}^{-1}(i\omega_n, \mathbf{p}) = \left(i\omega_n + \mu - \frac{\mathbf{p}^2}{2M}\right)\mathbf{1} - v_F \boldsymbol{\sigma}\cdot\mathbf{p}, \tag{9}$$

where the effective-mass parameter involved in the quadratic dispersion term arises from the next-to-nearest-neighbor hopping t' in the atomistic tight-binding Hamiltonian of graphene [20], $M = -2/(9a_0^2 t') \sim -1.36 \times 10^{-30}$ K g. On the other hand, we show that the self-energy in Eq. (6) can be reduced to the expression (see Appendix B)

$$\hat{\Sigma}(i\omega_n, \mathbf{p}) = n_{\text{dip}} \frac{e^2\mathcal{P}^2}{8\epsilon^2}\left[\mathbf{1}\,\mathcal{I}_1(i\omega_n, \mathbf{p}) + \frac{\boldsymbol{\sigma}\cdot\mathbf{p}}{p}\mathcal{I}_2(i\omega_n, \mathbf{p})\right], \tag{10}$$

where the exact definitions of the scalar functions $\mathcal{I}_1(i\omega_n, \mathbf{p})$ and $\mathcal{I}_2(i\omega_n, \mathbf{p})$ are given by Eq. (B4) in Appendix B. Consistently with the second-nearest-neighbor contribution in the graphene Hamiltonian, we consider only contributions up to second order in momentum in these integrals, such that

$$\begin{aligned} \mathcal{I}_1(i\omega_n, \mathbf{p}) &= \mathcal{I}_1^{(0)}(i\omega_n) + \mathbf{p}^2\mathcal{I}_1^{(2)}(i\omega_n) + O(\mathbf{p}^4), \\ \mathcal{I}_2(i\omega_n, \mathbf{p}) &= p\mathcal{I}_2^{(1)}(i\omega_n) + O(\mathbf{p}^3). \end{aligned} \tag{11}$$

Inserting the expression for the self-energy Eq. (10) and the bare inverse propagator Eq. (9) into the Dyson Eq. (7), we obtain the inverse full propagator

$$\begin{aligned} \hat{\Delta}_E^{-1} &= \left(i\omega_n + \mu - \frac{n_{\text{dip}}e^2\mathcal{P}^2}{8\epsilon^2}\mathcal{I}_1^{(0)}(i\omega_n) - \frac{\mathbf{p}^2}{2M}\left[1 + \frac{Mn_{\text{dip}}e^2\mathcal{P}^2}{4\epsilon^2}\mathcal{I}_1^{(2)}(i\omega_n)\right]\right)\mathbf{1} - \boldsymbol{\sigma}\cdot\mathbf{p}\, v_F\left(1 + \frac{n_{\text{dip}}e^2\mathcal{P}^2}{8\epsilon^2 v_F}\mathcal{I}_2^{(1)}(i\omega_n)\right) \\ &= z^{-1}\left\{\left(i\omega_n + \tilde{\mu} - \frac{\mathbf{p}^2}{2\tilde{M}}\right)\mathbf{1} - \boldsymbol{\sigma}\cdot\mathbf{p}\,\tilde{v}_F - \tilde{\Sigma}^{(2)}(\omega_n, \mathbf{p})\right\}. \end{aligned} \tag{12}$$

The fact that the tensor structure of the disorder-averaged propagator Eq. (12) is the same as the free one Eq. (9) supports the renormalized quasiparticle picture [22–24]. Therefore, after expanding at low frequencies with respect to the chemical potential, we defined the renormalized quasiparticle

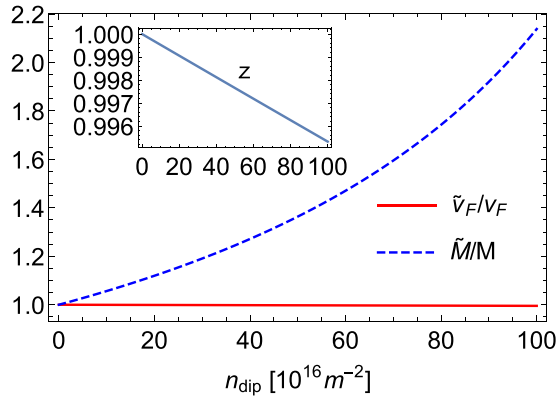

FIG. 3. Renormalized parameters $\tilde{M}/M$ (blue, dashed line) and $\tilde{v}_F/v_F$ (red, solid line), and renormalization factor z (inset) as a function of the concentration of adsorbed polar molecules $n_{\rm dip}$ (in units of 10^{16} m^{-2}).

parameters

$$\tilde{M}^{-1} = zM^{-1}\left(1 + \frac{Mn_{\rm dip}e^2\mathcal{P}^2}{4\epsilon^2}\mathrm{Re}\,\mathcal{I}_1^{(2)}(0)\right),$$
$$\tilde{\mu} = z\left(\mu - \frac{n_{\rm dip}e^2\mathcal{P}^2}{8\epsilon^2}\mathrm{Re}\,\mathcal{I}_1^{(0)}(0)\right),$$
$$\tilde{v}_F = zv_F\left(1 + \frac{n_{\rm dip}e^2\mathcal{P}^2}{8\epsilon^2 v_F}\mathrm{Re}\,\mathcal{I}_2^{(1)}(0)\right), \tag{13}$$

with the wave-function renormalization factor

$$z^{-1} = 1 - \frac{n_{\rm dip}e^2\mathcal{P}^2}{8\epsilon^2}\mathrm{Re}\,\frac{\partial}{\partial(i\omega)}\mathcal{I}_1^{(0)}\Big|_{\omega=0}, \tag{14}$$

while the matrix $\tilde{\Sigma}^{(2)}(\omega_n, \mathbf{p})$ contains the self-energy contributions at higher frequencies $O(\omega^2)$. Neglecting such higher-energy contributions, we therefore define the quasiparticle propagator

$$\tilde{\Delta}_E^{-1}(i\omega_n, \mathbf{p}) = \left(i\omega_n + \tilde{\mu} - \frac{\mathbf{p}^2}{2\tilde{M}}\right)\mathbf{1} - \boldsymbol{\sigma}\cdot\mathbf{p}\,\tilde{v}_F. \tag{15}$$

The dependence of the renormalized quasiparticle parameters defined in Eq. (13) on the adsorbed molecular concentration is presented in Fig. 3, where for illustration we have chosen the parameters for NH_3, with a dipole moment of $\mathcal{P} = 1.42$ D, and $a = 3.6$ Å.

These equations show that the disordered-averaged system under the presence of the adsorbed polar molecules can be reduced to an effective Lagrangian as in Eq. (1), but in terms of "free" renormalized quasiparticles defined by the scaled fermion fields $z^{-1/2}\psi(\mathbf{r})$, along with the renormalized parameters defined in Eq. (13). As usual in such a renormalization group (RG) procedure [25,26], Callan-Symanzik equations govern the flow of the renormalized n-point correlation vertices in parameter space as a function of a relevant energy scale Λ,

$$\tilde{\Gamma}^{(n)}(p_1, \ldots, p_n; \tilde{M}(\Lambda), \tilde{v}_F(\Lambda), \tilde{\mu}(\Lambda)) = z^{n/2}(\Lambda)\Gamma^{(n)}(p_1, \ldots, p_n; M, v_F, \mu), \tag{16}$$

where M, v_F, and μ represent the bare parameters, which are independent of the energy scale Λ. By applying the mathematical condition $d\Gamma^{(n)}(p_1, \ldots, p_n; M, v_F, \mu)/d\Lambda = 0$, the corresponding Callan-Symanzik equations are

$$\left[\Lambda\frac{\partial}{\partial\Lambda} + \beta(\tilde{v}_F)\frac{\partial}{\partial\tilde{v}_F} + \gamma_M\tilde{M}\frac{\partial}{\partial\tilde{M}} + \gamma_\mu\tilde{\mu}\frac{\partial}{\partial\tilde{\mu}} - n\gamma\right]\tilde{\Gamma}^{(n)} = 0, \tag{17}$$

where we defined the RG functions

$$\beta(\tilde{v}_F) = \frac{\partial\tilde{v}_F}{\partial\ln(\Lambda)}, \quad \gamma_M = \frac{\partial\ln(\tilde{M})}{\partial\ln(\Lambda)}, \quad \gamma_\mu = \frac{\partial\ln(\tilde{\mu})}{\partial\ln(\Lambda)},$$
$$\gamma = \frac{1}{2}\frac{\partial\ln(z)}{\partial\ln(\Lambda)}. \tag{18}$$

In our model, as clearly inferred from Eq. (13), the relevant energy scale that induces the RG flow is $\Lambda = en_{\rm dip}\mathcal{P}/\epsilon$, i.e., the electrostatic energy of the adsorbed polar molecules. In this language, Eq. (13) give the explicit solution of the RG flow equations at first-order in $\Lambda = en_{\rm dip}\mathcal{P}/\epsilon$. Therefore, the corresponding vertex functions in the renormalized quasiparticle effective theory, in particular for $n = 2$, are obtained by substituting $v_F \to \tilde{v}_F$, $M \to \tilde{M}$ into the definition of the "free" vertex functions [17]

$$\Gamma^k_{ab}(p; M, v_F) \to \tilde{\Gamma}^k_{ab}(p; \tilde{M}, \tilde{v}_F) = [\delta_{ab}p^k + 2\tilde{M}\tilde{v}_F[\sigma^k]_{ab}]. \tag{19}$$

Higher-order corrections to this vertex can be incorporated systematically [26] in terms of quasiparticle propagators in the spirit of contour-improved perturbation theory (CIPT) [27,28], also known as renormalized perturbation theory (RPT) [22,23] in condensed-matter systems. However, we shall neglect such higher-order contributions in our present analysis, under the assumption of relatively low molecular concentrations.

III. CONDUCTIVITY

From the Kubo linear response theory, the optical conductivity tensor is given by the expression [17,19]

$$\sigma_{kl}(\omega) = 4 \times \frac{\Pi^R_{kl}(p)}{i\omega}\Big|_{p=(\omega,0)}. \tag{20}$$

The retarded component of the polarization tensor is obtained via analytic continuation from the Euclidean, following the standard prescription $\Pi^R_{kl}(\omega, \mathbf{p}) = \Pi^E_{kl}(i\omega_n \to \omega + i\epsilon, \mathbf{p})$.

In our previous work, we have derived the expression of the Euclidean polarization tensor, which, in the present context, in terms of free renormalized quasiparticles reads [17,19]

$$\Pi^E_{kl}(i\omega_n, \mathbf{p}) = \frac{e^2}{4\tilde{M}^2}\frac{1}{\beta}\sum_{q_4=\omega_n, n\in\mathbb{Z}}\int\frac{d^2q}{(2\pi)^2}\tilde{\Gamma}^k_{ab}(p+2q) \times \tilde{\Delta}^E_{bc}(p+q)\tilde{\Gamma}^l_{cd}(p+2q)\tilde{\Delta}^E_{da}(q), \tag{21}$$

where the renormalized quasiparticle vertex $\tilde{\Gamma}^k_{ab}(p)$ was defined in Eq. (19).

Following the analysis in our previous work [17,19], we obtain that the tensor is symmetric and diagonal, $\sigma_{11} = \sigma_{22}$, $\sigma_{12} = \sigma_{21} = 0$. In particular, for the real part of the optical

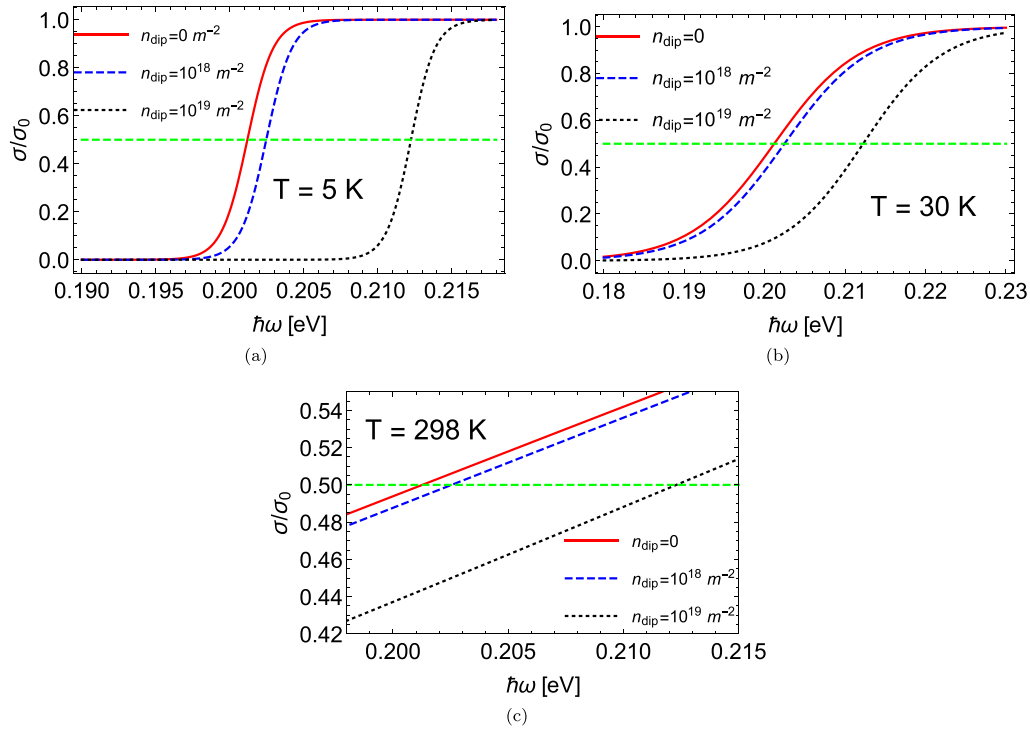

FIG. 4. Optical conductivity of graphene, calculated after Eq. (22) and normalized by the "universal" value $\sigma_0 = e^2/(4\hbar)$, as a function of frequency, for different adsorbed molecular concentrations $n_{\rm dip}$. We considered three temperatures (a) $T = 5$ K, (b) $T = 30$ K, and (c) $T = 298$ K, and a "bare" chemical potential $\mu = 0.1$ eV. The intercept with the horizontal dashed line corresponds to the center of each of the sigmoidal curves.

conductivity that can be measured in electronic transport experiments, we obtain the analytical expression [19]

$$\begin{aligned}&\mathrm{Re}\,\sigma_{11}(\omega,T)\\&=\frac{e^2}{8\hbar}\mathrm{sign}(\omega)\left\{\tanh\left[\frac{1}{2k_BT}\left(\frac{\hbar^2\omega^2}{8\tilde{M}\tilde{v}_F^2}+\frac{\hbar\omega}{2}-\tilde{\mu}\right)\right]\right.\\&\left.-\tanh\left[\frac{1}{2k_BT}\left(\frac{\hbar^2\omega^2}{8\tilde{M}\tilde{v}_F^2}-\frac{\hbar\omega}{2}-\tilde{\mu}\right)\right]\right\}.\end{aligned}\tag{22}$$

It is worth noting that an equivalent expression for the conductance can be obtained in the framework of standard perturbation theory by substituting the dressed propagators in Eq. (21), but keeping the bare vertices $\Gamma^k_{ab}(p;M,v_F)$. This alternative approach leads to an overall multiplicative factor $(zv_F/\tilde{v}_F)^2$ that only affects the definition of the zero-temperature limit of the conductance, but not the locus of the center of the sigmoidal. Moreover, it can be checked that this factor is nearly equal to 1 within the broad range of concentrations considered in this study, thus showing the equivalence of standard and renormalized perturbation theory results at this level. We notice that the zero-temperature limit of Eq. (22) reduces to the universal value $e^2/(4\hbar)$ as follows [19]:

$$\mathrm{Re}\,\sigma_{11}(\omega,T\to 0)=\begin{cases}\frac{e^2}{4\hbar}, & \frac{\hbar|\omega|}{2|\tilde{M}|\tilde{v}_F^2}>1-\sqrt{1-\frac{2\tilde{\mu}}{|\tilde{M}|\tilde{v}_F}},\\ 0 & \text{otherwise.}\end{cases}$$

In Fig. 4, we display the optical conductance, normalized by the "universal" value $\sigma_0 = e^2/(4\hbar)$, as a function of frequency for different molecular surface concentrations and three different temperatures: (a) $T = 5$ K, (b) $T = 30$ K, and (c) $T = 298$ K. For this example, we used the representative parameters of NH_3 and a chemical potential of $\mu = 0.1$ eV. A second example, but with a different chemical potential $\mu = 0.3$ eV, is displayed in Fig. 5. At any finite temperature, the center of the sigmoidal curve, represented in Figs. 4 and 5 by the intersection with the horizontal dashed line, is located at

$$\hbar\omega_{\rm center}=2|\tilde{M}|\tilde{v}_F^2\left(1-\sqrt{1-\frac{2\tilde{\mu}}{|\tilde{M}|\tilde{v}_F^2}}\right)\sim 2\tilde{\mu}+\frac{\tilde{\mu}^2}{|\tilde{M}|\tilde{v}_F^2}.\tag{23}$$

While temperature determines the steepness of the sigmoidal curve, we remark that the locus of this central point is independent of temperature, but it only depends on the chemical potential and the molecular surface concentration. In Fig. 6, we display the locus of this point as a function of the molecule surface concentration for the same representative parameters of NH_3 and two different values of the "bare" chemical potential: (a) $\mu = 0.1$ eV and (b) $\mu = 0.3$ eV, respectively. The inset in these figures displays the corresponding values for the renormalized chemical potential. In both cases, a change of about 6% is predicted from the model within the range of molecular concentrations displayed, independent of temperature. Although this change is proportionally small, it corresponds in absolute terms to ∼12 meV for the first case, and to ∼35 meV for the second case, which are experimentally detectable energy magnitudes. While the chemical potential values we chose here to illustrate the effect are relatively large, the simple relation [4] $\mu \sim \hbar v_F\sqrt{\pi n}$ indi-

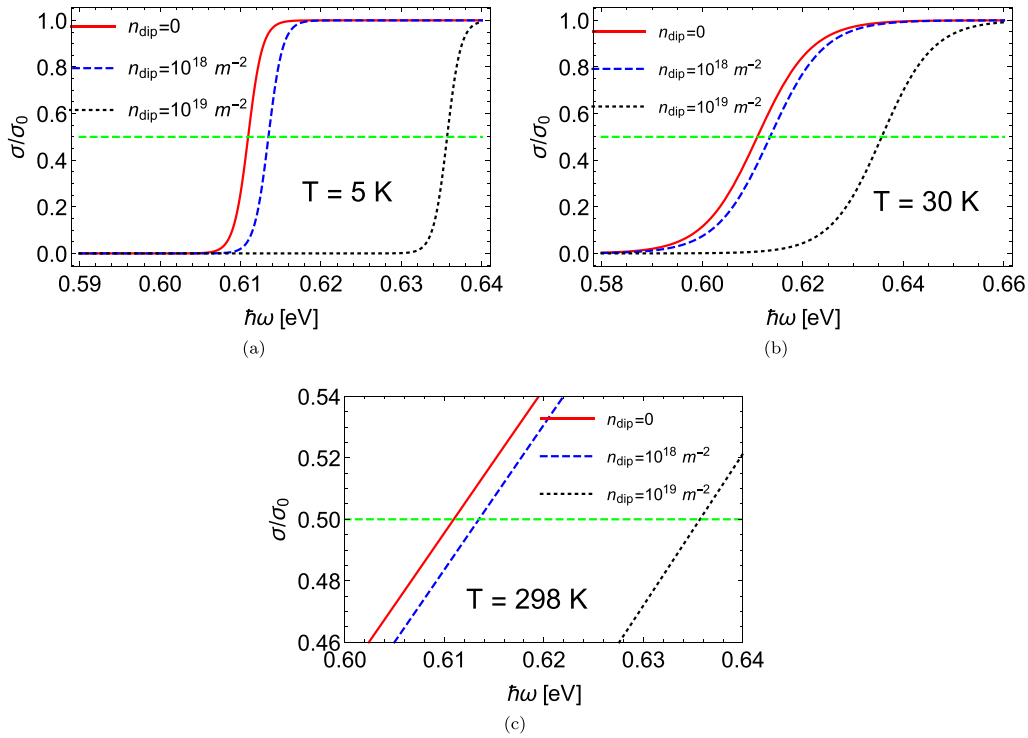

FIG. 5. Optical conductivity of graphene, calculated after Eq. (22) and normalized by the "universal" value $\sigma_0 = e^2/(4\hbar)$, as a function of frequency, for different adsorbed molecular concentrations $n_{\rm dip}$. We considered three temperatures (a) $T = 5$ K, (b) $T = 30$ K, and (c) $T = 298$ K, and a "bare" chemical potential $\mu = 0.3$ eV. The intercept with the horizontal dashed line corresponds to the center of each of the sigmoidal curves.

cates that $\mu \sim 0.1$–0.3 eV corresponds to electronic charge densities of the order of $n \sim (1 \times 10^{12})$–$(7 \times 10^{12})$ cm^{-2}. Indeed, electronic transport experiments in graphene have been performed with charge densities up to an order of magnitude higher than these values [29], and the measured resistivity curves are fully compatible with the Dirac effective theory [4,29].

IV. CONCLUSION

We developed a quantum field theory that describes the effects of different concentrations of adsorbed polar molecules on the optical conductivity of graphene, at finite temperature and chemical potential. Our analytical results show that from electric transport measurements at finite frequency, it is possible to read the shift in the conductivity curve [defined as $\omega_{\rm center}$ in Eq. (23)]. From this value, which is temperature-independent, as illustrated in the examples displayed in Fig. 6, it is possible to estimate the molecular surface concentration, since it determines the renormalized parameters $\tilde{\mu}$, $\tilde{M}$, and $\tilde{v}_F$ in terms of the "bare" graphene parameters M and v_F, as well as the actual chemical potential μ, through the analytical Eqs. (13) and (14). Finally, it is worth noticing that the quadratic term in the dispersion relation of quasiparti-

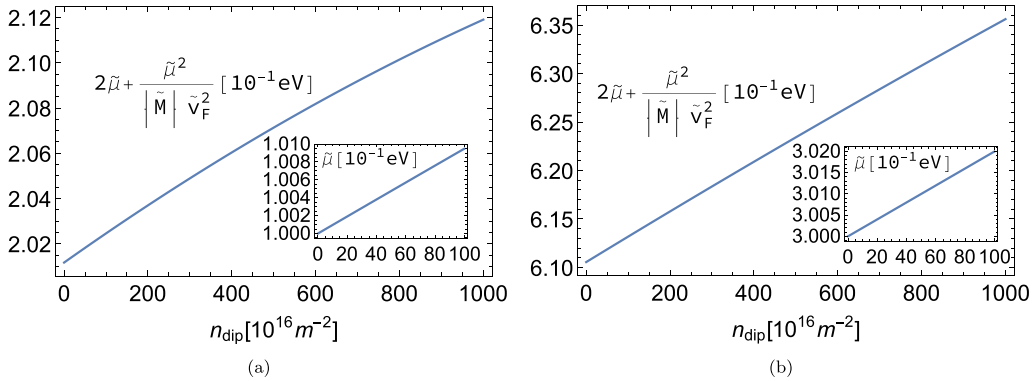

FIG. 6. The locus of the center of the sigmoidal conductance curve defined in Eq. (23) (main figure), and renormalized chemical potential (inset), as a function of adsorbed molecular concentration $n_{\rm dip}$. The "bare" chemical potential is set to (a) $\mu = 0.1$ eV and (b) $\mu = 0.3$ eV, respectively.

cles is induced by the adsorbed dipoles even in the $M \to \infty$ limit (which corresponds to the linear model of graphene) as follows from the first line in Eq. (13) and Eq. (B12) in Appendix B.

ACKNOWLEDGMENTS

H.F. is partially supported by CONICET (Argentina), and acknowledges support from UNLP through Proy. Nro. 11/X909 (Argentina). M.L. acknowledges support from ANID/PIA/Basal (Chile) under Grant No. FB082, Fondecyt Regular Grant No. 1190192, and Fondecyt Regular Grant No. 1170107. E.M. acknowledges financial support from the Fondecyt Regular Grant No. 1190361, and from Project Grant ANID PIA Anillo ACT192023. E.M. and M.L also acknowledge financial support from Fondecyt Regular Grant No. 1200483.

APPENDIX A

In this Appendix, we present the basic considerations involved in the disorder averaging that leads to the noncrossing approximation (NCA) applied in this work. This analysis closely follows Ref. [21]. We start by considering the potential experienced at site $\mathbf{r} \in \mathbb{R}^2$, due to the presence of an ensemble of N polar molecules adsorbed over the graphene surface with a total area A, such that the surface concentration is $n_{\rm dip} = N/A$. The position of the center of mass of each molecule is at $(\mathbf{R}_j, a)$, with $a > 0$ the height with respect to the graphene surface (at $z = 0$) and $\mathbf{R}_j \in \mathbb{R}^2$ the position over the plane, for $1 \leqslant j \leqslant N$. The corresponding potential is

$$V(\mathbf{r}) = \sum_{j=1}^{N} V_{\boldsymbol{d}_j}(\mathbf{r} - \mathbf{R}_j), \tag{A1}$$

where, as displayed in the main text, the potential for each dipole is

$$V_{\mathbf{d}_j}(\mathbf{r}) = \frac{\mathcal{P}}{4\pi\epsilon d}\left(\frac{1}{\sqrt{(\mathbf{r} - \frac{\mathbf{d}_j}{2})^2 + a^2}} - \frac{1}{\sqrt{(\mathbf{r} + \frac{\mathbf{d}_j}{2})^2 + a^2}}\right). \tag{A2}$$

The 2D Fourier transform of this potential is given by the expression

$$\begin{aligned}\hat{V}_{\mathbf{d}_j}(\mathbf{q}) &= \int_{\mathbb{R}^2} d^2r\, e^{i\mathbf{q}\cdot\mathbf{r}} V_{\mathbf{d}_j}(\mathbf{r}) \\ &= \frac{i\mathcal{P}\sin\left(\frac{\mathbf{q}\cdot\mathbf{d}_j}{2}\right)}{2\pi\epsilon d}\int_0^\infty dr \frac{r}{\sqrt{r^2+a^2}}\int_0^{2\pi} d\phi\, e^{iqr\cos(\phi)} \\ &= \frac{i\mathcal{P}\sin\left(\frac{\mathbf{q}\cdot\mathbf{d}_j}{2}\right)}{\epsilon d}\int_0^\infty dr \frac{rJ_0(qr)}{\sqrt{r^2+a^2}} \\ &= \frac{i\mathcal{P}\sin\left(\frac{\mathbf{q}\cdot\mathbf{d}_j}{2}\right)}{\epsilon q d} e^{-qa}.\end{aligned} \tag{A3}$$

In the strict dipole approximation, i.e., $d \to 0$ but $\mathcal{P}_j$ finite, the Fourier transform reduces to the simpler expression

$$\lim_{d\to 0} \hat{V}_{\mathbf{d}_j}(\mathbf{q}) \equiv \hat{V}_{\boldsymbol{\mathcal{P}}_j}(\mathbf{q}) = \frac{i\mathbf{q}\cdot\boldsymbol{\mathcal{P}}_j}{2\epsilon q} e^{-qa}. \tag{A4}$$

With this result, the 2D Fourier transform of the potential is given by

$$\begin{aligned}\hat{V}(\mathbf{q}) &= \int_{\mathbb{R}^2} d^2r\, e^{i\mathbf{q}\cdot\mathbf{r}} V(\mathbf{r}) \\ &= \sum_{j=1}^{N}\int_{\mathbb{R}^2} d^2r\, e^{i\mathbf{q}\cdot\mathbf{r}} V_{\boldsymbol{d}_j}(\mathbf{r} - \mathbf{R}_j) \\ &= \sum_{j=1}^{N} e^{i\mathbf{q}\cdot\mathbf{R}_j}\int_{\mathbb{R}^2} d^2r\, e^{i\mathbf{q}\cdot\mathbf{r}} V_{\boldsymbol{d}_j}(\mathbf{r}) \\ &= \sum_{j=1}^{N} \hat{V}_{\boldsymbol{d}_j}(\mathbf{q}) e^{i\mathbf{q}\cdot\mathbf{R}_j} \xrightarrow{d\to 0} \sum_{j=1}^{N} \hat{V}_{\boldsymbol{\mathcal{P}}_j}(\mathbf{q}) e^{i\mathbf{q}\cdot\mathbf{R}_j}.\end{aligned} \tag{A5}$$

We shall assume that the positions of the adsorbed molecules over the graphene surface, i.e., the set $\{\mathbf{R}_j\}_{j=1}^N$, as well as the orientation of the dipole moments $\{\boldsymbol{\mathcal{P}}_j\}_{j=1}^N$ are independent and identically distributed random variables. Therefore, writing $\boldsymbol{\mathcal{P}}_j = \mathcal{P}(\cos(\varphi_j), \sin(\varphi_j))$, with $\varphi_j \in [0, 2\pi]$ a uniformly distributed random variable, we have that the average dipole moment is

$$\langle \boldsymbol{\mathcal{P}}_j \rangle = \mathcal{P}(\langle\cos(\varphi_j)\rangle, \langle\sin(\varphi_j)\rangle) = 0, \tag{A6}$$

and hence the average of a single Fourier component of the potential also vanishes,

$$\langle \hat{V}_{\boldsymbol{\mathcal{P}}_j}(\mathbf{q})\rangle = \frac{ie^{-qa}}{2\epsilon q}\mathbf{q}\cdot\langle\boldsymbol{\mathcal{P}}_j\rangle = 0. \tag{A7}$$

Similarly, for $\mathbf{q}_1 = q_1(\cos(\phi_1), \sin(\phi_1))$ and $\mathbf{q}_2 = q_2(\cos(\phi_2), \sin(\phi_2))$, we obtain the following for the disorder-averaged product of a pair of Fourier components of the potential:

$$\begin{aligned}&\langle \hat{V}_{\boldsymbol{\mathcal{P}}_j}(\mathbf{q}_1)\hat{V}_{\boldsymbol{\mathcal{P}}_{j'}}(\mathbf{q}_2)\rangle \\ &\quad= \frac{i^2e^{-(q_1+q_2)a}}{4\epsilon^2 q_1 q_2}\langle \mathbf{q}_1\cdot\boldsymbol{\mathcal{P}}_j\mathbf{q}_2\cdot\boldsymbol{\mathcal{P}}_{j'}\rangle \\ &\quad= \frac{i^2e^{-(q_1+q_2)a}\mathcal{P}^2}{4\epsilon^2}(\cos\phi_1\cos\phi_2\langle\cos\varphi_j\cos\varphi_{j'}\rangle \\ &\qquad+ \sin\phi_1\sin\phi_2\langle\sin\varphi_j\sin\varphi_{j'}\rangle + \cos\phi_1\sin\phi_2 \\ &\qquad\times\langle\cos\varphi_j\sin\varphi_{j'}\rangle + \sin\phi_1\cos\phi_2\langle\cos\varphi_j\sin\varphi_{j'}\rangle) \\ &\quad= \frac{i^2e^{-(q_1+q_2)a}\mathcal{P}^2}{8\epsilon^2}\delta_{j,j'}(\cos\phi_1\cos\phi_2 + \sin\phi_1\sin\phi_2) \\ &\quad= \delta_{j,j'}\frac{i^2e^{-(q_1+q_2)a}\mathcal{P}^2}{8\epsilon^2}\frac{\mathbf{q}_1\cdot\mathbf{q}_2}{q_1q_2}.\end{aligned} \tag{A8}$$

Generalizing this procedure, it is straightforward to show that the average over orientations of the product of an odd number of potential terms is identically zero,

$$\langle \hat{V}_{\boldsymbol{\mathcal{P}}_{j_1}}(\mathbf{q}_1)\hat{V}_{\boldsymbol{\mathcal{P}}_{j_2}}(\mathbf{q}_2)\cdots\hat{V}_{\boldsymbol{\mathcal{P}}_{j_{2n+1}}}(\mathbf{q}_{2n+1})\rangle = 0, \tag{A9}$$

since

$$\begin{aligned}\langle\cos(\varphi_{j_1})\cos(\varphi_{j_2})\cdots\cos(\varphi_{j_{2n+1}})\rangle &= 0, \\ \langle\sin(\varphi_{j_1})\sin(\varphi_{j_2})\cdots\sin(\varphi_{j_{2n+1}})\rangle &= 0.\end{aligned} \tag{A10}$$

On the other hand, the statistical average over orientations of the product of an even number of potential terms does

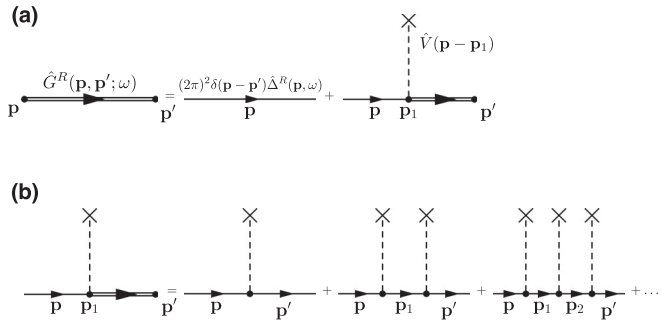

FIG. 7. (a) Feynman diagrams for the self-consistent Lippmann-Schwinger series that determines the retarded Green's function under an external scattering potential in Eq. (A14). (b) Expansion of the infinite series generated by the scattering diagram described in (a).

not vanish, but it factors into all possible products of pair correlators (contractions) as defined in Eq. (A8),

$$\langle \hat{V}_{\mathcal{P}_{j_1}}(\mathbf{q}_1)\hat{V}_{\mathcal{P}_{j_2}}(\mathbf{q}_2)\cdots\hat{V}_{\mathcal{P}_{j_{2n+1}}}(\mathbf{q}_{2n+1})\rangle = \text{all contractions}. \tag{A11}$$

For instance, consider the average over a product of four potential terms that factors into three different contractions,

$$\begin{aligned}
&\langle \hat{V}_{\mathcal{P}_{j_1}}(\mathbf{q}_1)\hat{V}_{\mathcal{P}_{j_2}}(\mathbf{q}_2)\hat{V}_{\mathcal{P}_{j_3}}(\mathbf{q}_3)\hat{V}_{\mathcal{P}_{j_4}}(\mathbf{q}_4)\rangle \\
&\quad = \delta_{j_1,j_2}\delta_{j_3,j_4}\langle \hat{V}_{\mathcal{P}_{j_1}}(\mathbf{q}_1)\hat{V}_{\mathcal{P}_{j_1}}(\mathbf{q}_2)\rangle\langle \hat{V}_{\mathcal{P}_{j_3}}(\mathbf{q}_3)\hat{V}_{\mathcal{P}_{j_3}}(\mathbf{q}_4)\rangle \\
&\qquad + \delta_{j_1,j_4}\delta_{j_2,j_3}\langle \hat{V}_{\mathcal{P}_{j_1}}(\mathbf{q}_1)\hat{V}_{\mathcal{P}_{j_1}}(\mathbf{q}_4)\rangle\langle \hat{V}_{\mathcal{P}_{j_2}}(\mathbf{q}_2)\hat{V}_{\mathcal{P}_{j_2}}(\mathbf{q}_3)\rangle \\
&\qquad + \delta_{j_1,j_3}\delta_{j_2,j_4}\langle \hat{V}_{\mathcal{P}_{j_1}}(\mathbf{q}_1)\hat{V}_{\mathcal{P}_{j_1}}(\mathbf{q}_3)\rangle\langle \hat{V}_{\mathcal{P}_{j_2}}(\mathbf{q}_2)\hat{V}_{\mathcal{P}_{j_2}}(\mathbf{q}_4)\rangle.
\end{aligned} \tag{A12}$$

Similarly, for the average over the molecular positions $\mathbf{R}_j$, we have

$$\langle e^{i(\mathbf{q}-\mathbf{q}')\cdot\mathbf{R}_j}\rangle = \frac{1}{A}\int_{\mathbb{R}^2} d^2R_j e^{i(\mathbf{q}-\mathbf{q}')\cdot\mathbf{R}_j} = \frac{(2\pi)^2}{A}\delta(\mathbf{q}-\mathbf{q}'). \tag{A13}$$

Let us now consider the Lippmann-Schwinger series, in momentum space, for the scattering process across a given realization of the ensemble of adsorbed molecules. This can be written in closed form in terms of the self-consistent integral equation for the retarded Green's function $\hat{G}^R(\mathbf{p},\mathbf{p}';\omega)$,

$$\begin{aligned}
\hat{G}^R(\mathbf{p},\mathbf{p}';\omega) &= (2\pi)^2\delta(\mathbf{p}-\mathbf{p}')\hat{\Delta}_0^R(\mathbf{p},\omega) + \hat{\Delta}_0^R(\mathbf{p},\omega) \\
&\quad\times\int\frac{d^2p_1}{(2\pi)^2}e\hat{V}(\mathbf{p}-\mathbf{p}_1)\hat{G}^R(\mathbf{p}_1,\mathbf{p}';\omega),
\end{aligned} \tag{A14}$$

where the "free" retarded Green's function is trivially translationally invariant and hence diagonal in momentum space,

$$\hat{G}_0^R(\mathbf{p},\mathbf{p}';\omega) = (2\pi)^2\delta(\mathbf{p}-\mathbf{p}')\hat{\Delta}_0^R(\mathbf{p},\omega). \tag{A15}$$

This equation can be expressed diagrammatically as depicted in Fig. 7(a), where the scattering term represents an expansion over a series including all possible numbers of individual scattering events, as depicted diagrammatically in Fig. 7(b). In these Feynman diagrams, the double line represents the retarded Green's function $\hat{G}^R(\mathbf{p},\mathbf{p}';\omega)$, while the single line represents the "free" retarded Green's function defined in Eq. (A15), and the dashed lines with a cross on top represent potential scattering terms $\hat{V}(\mathbf{p}-\mathbf{p}_1)$.

We perform a statistical average over the disordered distribution of positions and dipole orientations in Eq. (A14) to obtain the series [see Fig. 7(b)]

$$\begin{aligned}
\langle\hat{G}^R(\mathbf{p},\mathbf{p}';\omega)\rangle &= (2\pi)^2\delta(\mathbf{p}-\mathbf{p}')\hat{\Delta}_0^R(\mathbf{p},\omega) + \hat{\Delta}_0^R(\mathbf{p},\omega)\int\frac{d^2p_1}{(2\pi)^2}\langle e\hat{V}(\mathbf{p}-\mathbf{p}_1)\hat{G}^R(\mathbf{p}_1,\mathbf{p}';\omega)\rangle \\
&= (2\pi)^2\delta(\mathbf{p}-\mathbf{p}')\hat{\Delta}_0^R(\mathbf{p},\omega) + \hat{\Delta}_0^R(\mathbf{p},\omega)\langle e\hat{V}(\mathbf{p}-\mathbf{p}')\rangle\hat{\Delta}_0^R(\mathbf{p}',\omega) \\
&\quad + \hat{\Delta}_0^R(\mathbf{p},\omega)\int\frac{d^2p_1}{(2\pi)^2}\langle e^2\hat{V}(\mathbf{p}-\mathbf{p}_1)\hat{V}(\mathbf{p}_1-\mathbf{p}')\rangle\hat{\Delta}_0^R(\mathbf{p}_1,\omega)\hat{\Delta}_0^R(\mathbf{p}',\omega)+\cdots.
\end{aligned} \tag{A16}$$

To analyze this series expansion, we need to consider the statistical averages of the Fourier components of the potential, as well as of their products at different orders. Notice that the disorder average of the potential, under the assumptions of statistical independence of the parameters, is

$$\begin{aligned}
\langle\hat{V}(\mathbf{p}-\mathbf{p}')\rangle &= \sum_{j=1}^{N}\langle e^{i(\mathbf{p}-\mathbf{p}')\cdot\mathbf{R}_j}\rangle\langle\hat{V}_{\mathcal{P}_j}(\mathbf{p}-\mathbf{p}')\rangle \\
&= \frac{N}{A}(2\pi)^2\delta(\mathbf{p}-\mathbf{p}')\langle\hat{V}_{\mathcal{P}_j}(0)\rangle \\
&= 0,
\end{aligned} \tag{A17}$$

where in the second line we applied Eq. (A13), and in the last step we used Eq. (A7). Therefore, clearly this first correction vanishes after averaging over dipole moment orientations. Moreover, as a consequence of Eq. (A9), all the averages involving a product of an odd number of potential terms will vanish, as depicted in Fig. 8(a), while those involving an even number will remain finite.

Let us now consider the second-order contribution,

$$\begin{aligned}
&\langle e^2\hat{V}(\mathbf{p}-\mathbf{p}_1)\hat{V}(\mathbf{p}_1-\mathbf{p}')\rangle \\
&\quad = \sum_{j=1}^{N}\langle e^{i(\mathbf{p}-\mathbf{p}')\cdot\mathbf{R}_j}\rangle\langle e^2\hat{V}_{\mathcal{P}_j}(\mathbf{p}-\mathbf{p}_1)\hat{V}_{\mathcal{P}_j}(\mathbf{p}_1-\mathbf{p}')\rangle \\
&\quad = \frac{N}{A}(2\pi)^2\delta(\mathbf{p}-\mathbf{p}')\frac{e^2\mathcal{P}^2}{8\epsilon^2}e^{-2a|\mathbf{p}-\mathbf{p}_1|} \\
&\quad = (2\pi)^2\delta(\mathbf{p}-\mathbf{p}')n_{\text{dip}}|\hat{V}_{\text{avg}}(\mathbf{p}-\mathbf{p}_1)|^2,
\end{aligned} \tag{A18}$$

where $n_{\text{dip}} = N/A$ is the molecular surface concentration. We remark that this contribution is explicitly diagonal in momentum. This term is represented diagrammatically in Fig. 8(b),

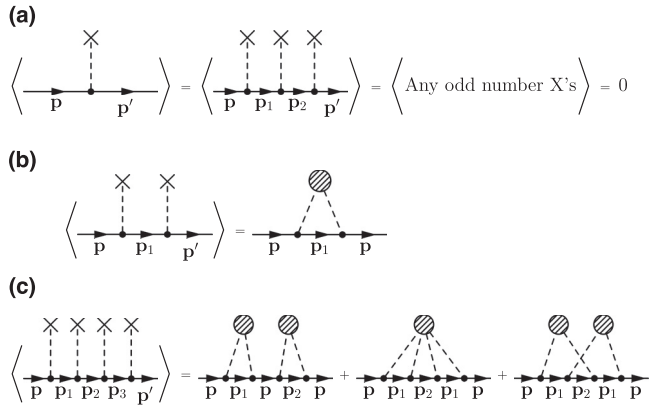

FIG. 8. (a) Statistical average over the random scattering potential represented by an odd number of X's in each diagram. (b) Statistical average over the scattering potential in the diagram with two X's, as calculated in detail in the main text. (c) Statistical average over the scattering potential in the diagram with four X's, that leads to three subsequent diagrams.

where the averaging process in Eq. (A18) is graphically described as pairing the crosses into a single blob. Therefore, from this result we obtain that the second-order contribution to the averaged retarded propagator, as depicted in Fig. 8(b), corresponds to the expression

$$\langle \hat{G}^{(2)}(\mathbf{p},\mathbf{p}';\omega)\rangle = (2\pi)^2\delta(\mathbf{p}-\mathbf{p}')\hat{\Delta}_0^R(\mathbf{p},\omega) \times n_{\rm dip}\int \frac{d^2p_1}{(2\pi)^2}|\hat{V}_{\rm avg}(\mathbf{p}-\mathbf{p}_1)|^2\hat{\Delta}_0^R(\mathbf{p}_1,\omega) \times \hat{\Delta}_0^R(\mathbf{p},\omega), \tag{A19}$$

where we defined the disordered-averaged potential energy

$$|\hat{V}_{\rm avg}(\mathbf{p})|^2 = \frac{e^2\mathcal{P}^2}{8\epsilon^2}e^{-2a|\mathbf{p}|}. \tag{A20}$$

As a final explicit example, let us consider the next nonvanishing contribution corresponding to the fourth-order diagram depicted in Fig. 8(c). This term involves the statistical average over a product of four potential scattering terms, which according to Eq. (A12) leads to three terms involving pairing contractions,

$$\langle e^4\hat{V}(\mathbf{p}-\mathbf{p}_1)\hat{V}(\mathbf{p}_1-\mathbf{p}_2)\hat{V}(\mathbf{p}_2-\mathbf{p}_3)\hat{V}(\mathbf{p}_3-\mathbf{p}')\rangle = C_1+C_2+C_3. \tag{A21}$$

The term C_1, following Eq. (A12), involves the pairings $\delta_{j_1,j_2}\delta_{j_3,j_4}$, in correspondence to the first diagram on the right in Fig. 8(c) that lumps the corresponding crosses into blobs. The algebraic expression is

$$C_1 = \sum_{j_1,j_3}\langle e^{i\mathbf{R}_{j_1}\cdot(\mathbf{p}-\mathbf{p}_2)}\rangle\langle e^{i\mathbf{R}_{j_3}\cdot(\mathbf{p}_2-\mathbf{p}')}\rangle\langle\hat{V}_{\mathcal{P}_{j_1}}(\mathbf{p}-\mathbf{p}_1) \times\hat{V}_{\mathcal{P}_{j_1}}(\mathbf{p}_1-\mathbf{p}_2)\rangle\langle\hat{V}_{\mathcal{P}_{j_3}}(\mathbf{p}_2-\mathbf{p}_3)\hat{V}_{\mathcal{P}_{j_3}}(\mathbf{p}_3-\mathbf{p}')\rangle = (2\pi)^4\delta(\mathbf{p}-\mathbf{p}_2)\delta(\mathbf{p}_2-\mathbf{p}')n_{\rm dip}^2|\hat{V}_{\rm avg}(\mathbf{p}-\mathbf{p}_1)|^2 \times|\hat{V}_{\rm avg}(\mathbf{p}_3-\mathbf{p}')|^2, \tag{A22}$$

where we used Eq. (A13), and the definition in Eq. (A20). The term C_2, following Eq. (A12), involves the pairings $\delta_{j_1,j_4}\delta_{j_2,j_3}$, in correspondence to the second diagram on the right in Fig. 8(c) that lumps the corresponding crosses into blobs. The algebraic expression is

$$C_2 = \sum_{j_1,j_2}\langle e^{i\mathbf{R}_{j_1}\cdot(\mathbf{p}-\mathbf{p}_1+\mathbf{p}_3-\mathbf{p}')}\rangle\langle e^{i\mathbf{R}_{j_2}\cdot(\mathbf{p}_2-\mathbf{p}_3+\mathbf{p}_1-\mathbf{p}_2)}\rangle \times\langle\hat{V}_{\mathcal{P}_{j_1}}(\mathbf{p}-\mathbf{p}_1)\hat{V}_{\mathcal{P}_{j_1}}(\mathbf{p}_3-\mathbf{p}')\rangle \times\langle\hat{V}_{\mathcal{P}_{j_2}}(\mathbf{p}_1-\mathbf{p}_2)\hat{V}_{\mathcal{P}_{j_2}}(\mathbf{p}_2-\mathbf{p}_3)\rangle = (2\pi)^4\delta(\mathbf{p}-\mathbf{p}'+\mathbf{p}_3-\mathbf{p}_1)\delta(\mathbf{p}_1-\mathbf{p}_3) \times n_{\rm dip}^2|\hat{V}_{\rm avg}(\mathbf{p}-\mathbf{p}_1)|^2|\hat{V}_{\rm avg}(\mathbf{p}_1-\mathbf{p}_2)|^2, \tag{A23}$$

where we used Eq. (A13) and the definition in Eq. (A20). Finally, the term C_3, following Eq. (A12), involves the pairings $\delta_{j_1,j_3}\delta_{j_2,j_4}$, in correspondence to the third diagram on the right-hand side in Fig. 8(c) that lumps the corresponding crosses into blobs. The algebraic expression is

$$C_3 = \sum_{j_1,j_2}\langle e^{i\mathbf{R}_{j_1}\cdot(\mathbf{p}-\mathbf{p}_1+\mathbf{p}_2-\mathbf{p}_3)}\rangle\langle e^{i\mathbf{R}_{j_2}\cdot(\mathbf{p}_1-\mathbf{p}_2+\mathbf{p}_3-\mathbf{p}')}\rangle \times\langle\hat{V}_{\mathcal{P}_{j_1}}(\mathbf{p}-\mathbf{p}_1)\hat{V}_{\mathcal{P}_{j_1}}(\mathbf{p}_2-\mathbf{p}_3)\rangle \times\langle\hat{V}_{\mathcal{P}_{j_2}}(\mathbf{p}_1-\mathbf{p}_2)\hat{V}_{\mathcal{P}_{j_2}}(\mathbf{p}_3-\mathbf{p}')\rangle = (2\pi)^4\delta(\mathbf{p}-\mathbf{p}_1+\mathbf{p}_2-\mathbf{p}_3)\delta(\mathbf{p}_1-\mathbf{p}_2+\mathbf{p}_3-\mathbf{p}') \times n_{\rm dip}^2|\hat{V}_{\rm avg}(\mathbf{p}-\mathbf{p}_1)|^2|\hat{V}_{\rm avg}(\mathbf{p}_1-\mathbf{p}_2)|^2. \tag{A24}$$

Integrating expressions C_1, C_2, and C_3, we obtain the fourth-order contribution corresponding to the diagram in Fig. 8(c),

$$\langle\hat{G}^{(4)}(\mathbf{p},\mathbf{p}';\omega)\rangle = \hat{\Delta}_0^R(\mathbf{p},\omega)\int\frac{d^2p_1}{(2\pi)^2}\int\frac{d^2p_2}{(2\pi^2)}\int\frac{d^2p_3}{(2\pi)^2} \times[C_1+C_2+C_3]\hat{\Delta}_0^R(\mathbf{p}_1,\omega)\hat{\Delta}_0^R(\mathbf{p}_2,\omega)\hat{\Delta}_0^R(\mathbf{p}_3,\omega)$$

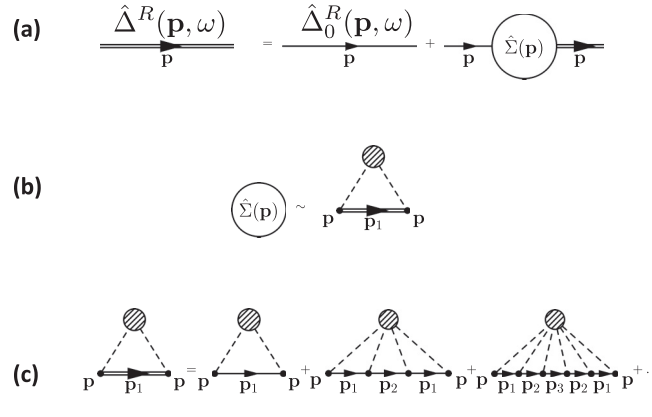

FIG. 9. (a) The Dyson equation for the average retarded propagator, with the one-particle irreducible self-energy represented by the open symbol $\hat{\Sigma}(\mathbf{p})$. (b) We adopt the NCA, as explained in the main text. (c) The infinite expansion represented by the diagrams contributing to the average one-particle irreducible self-energy in the NCA.

$$\times \hat{\Delta}_0^R(\mathbf{p}', \omega)$$

$$= (2\pi)^2 \delta(\mathbf{p} - \mathbf{p}') \hat{\Delta}_0^R(\mathbf{p}, \omega) \hat{\Sigma}^{(4)}(\mathbf{p}, \omega) \hat{\Delta}_0^R(\mathbf{p}, \omega), \quad \text{(A25)}$$

which, as Eq. (A19), is clearly diagonal in momentum space, and we defined the "self-energy" contributions according to the three diagrams on the right-hand side of Fig. 8(c),

$$\hat{\Sigma}^{(4)}(\mathbf{p}, \omega) = \hat{\Sigma}_1^{(4)}(\mathbf{p}, \omega) + \hat{\Sigma}_2^{(4)}(\mathbf{p}, \omega) + \hat{\Sigma}_3^{(4)}(\mathbf{p}, \omega). \quad \text{(A26)}$$

While $\hat{\Sigma}_1^{(4)}(\mathbf{p}, \omega)$ represents a reducible diagram, given by the iteration of the irreducible diagram in Fig. 8(b), the term $\hat{\Sigma}_2^{(4)}(\mathbf{p}, \omega)$ represents an irreducible diagram of second order, and so does the third diagram $\hat{\Sigma}_3^{(4)}(\mathbf{p}, \omega)$.

Performing this procedure to all orders, the resulting exact expression for the disorder-averaged propagator can be written in closed form as a Dyson equation, as depicted diagrammatically in Fig. 9(a),

$$\hat{\Delta}^R(\mathbf{p}, \omega) = \hat{\Delta}_0^R(\mathbf{p}, \omega) + \hat{\Delta}_0^R(\mathbf{p}, \omega) \hat{\Sigma}(\omega, \mathbf{p}) \hat{\Delta}^R(\mathbf{p}, \omega), \quad \text{(A27)}$$

where $\hat{\Sigma}(\omega, \mathbf{p})$ represents the one-particle irreducible self-energy. In what follows, we shall adopt the NCA [21], as indicated in Fig. 9(b), by neglecting diagrams where the potential lines cross [as, for instance, $\hat{\Sigma}_3^{(4)}(\mathbf{p}, \omega)$ in Fig. 8(c)], which allows us to perform a resummation of the infinite series of diagrams depicted in Fig. 9(b). The corresponding NCA irreducible self-energy is therefore defined by

$$\hat{\Sigma}(\omega, \mathbf{p}) = n_{\text{dip}} \int \frac{d^2q}{(2\pi)^2} |\hat{V}_{\text{avg}}(\mathbf{p} - \mathbf{q})|^2 \hat{\Delta}^R(\omega, \mathbf{q}), \quad \text{(A28)}$$

with $|\hat{V}_{\text{avg}}(\mathbf{p} - \mathbf{q})|^2$ defined in Eq. (A20).

APPENDIX B

In this Appendix, we present the calculation of the self-energy coefficients $\mathcal{I}_1(i\omega_n, \mathbf{p})$ and $\mathcal{I}_2(i\omega_n, \mathbf{p})$, as defined in the main text. We start by considering the self-energy in Eq. (A28), and, for low molecular concentrations, we substitute in the integral the expression for the free propagator,

$$\hat{\Delta}^R(\mathbf{q}, \omega) \to \hat{\Delta}_0^R(\mathbf{q}, \omega) = \frac{i\omega_n + \mu - \frac{\mathbf{q}^2}{2M} + v_F \boldsymbol{\sigma} \cdot \mathbf{q}}{\left(i\omega_n + \mu - \frac{q^2}{2M}\right)^2 - v_F^2 q^2}. \quad \text{(B1)}$$

By defining the coordinates $\mathbf{p} = p(\cos\varphi, \sin\varphi)$ and $\mathbf{q} = q(\cos(\theta - \varphi), \sin(\theta - \varphi))$, we have

$$\mathbf{q} \cdot \boldsymbol{\sigma} = q \begin{pmatrix} 0 & e^{-i(\theta-\varphi)} \\ e^{i(\theta-\varphi)} & 0 \end{pmatrix}, \quad \text{(B2)}$$

such that the self-energy in Eq. (A28) is given by the expression

$$\hat{\Sigma}(i\omega_n, \mathbf{p}) = n_{\text{dip}} \frac{e^2 \mathcal{P}^2}{8\epsilon^2} \left(\mathbf{1}\, \mathcal{I}_1(i\omega_n, \mathbf{p}) + \frac{\boldsymbol{\sigma} \cdot \mathbf{p}}{p} \mathcal{I}_2(i\omega_n, \mathbf{p}) \right), \quad \text{(B3)}$$

where we defined the integrals

$$\mathcal{I}_1(i\omega_n, \mathbf{p}) = \int \frac{d^2q}{(2\pi)^2} \frac{e^{-2|\mathbf{p}-\mathbf{q}|a} \left(i\omega_n + \mu - \frac{q^2}{2M}\right)}{\left(i\omega_n + \mu - \frac{q^2}{2M}\right)^2 - v_F^2 q^2}, \quad \mathcal{I}_2(i\omega_n, \mathbf{p}) = \int \frac{d^2q}{(2\pi)^2} \frac{e^{-2|\mathbf{p}-\mathbf{q}|a} q e^{\pm i\theta}}{\left(i\omega_n + \mu - \frac{q^2}{2M}\right)^2 - v_F^2 q^2}. \quad \text{(B4)}$$

Here we use polar coordinates $d^2q = q\, dq\, d\theta$, $\theta \in [0, 2\pi)$, and $q \in [0, \infty)$. To evaluate those integrals, we perform a series expansion in powers of the external momentum $\mathbf{p}$, retaining up to second order consistently with the next-to-nearest-neighbor approximation in the graphene Hamiltonian [20]. Therefore, for the first integral we have

$$\mathcal{I}_1(i\omega_n, \mathbf{p}) = \mathcal{I}_1^{(0)}(i\omega_n) + \mathbf{p}^2\, \mathcal{I}_1^{(2)}(i\omega_n) + O\left(p^4\right), \quad \text{(B5)}$$

where

$$\begin{aligned} \mathcal{I}_1^{(0)}(i\omega) = &-\frac{\mu + i\omega}{8\pi {v_F}^2} \left\{ e^{-\frac{2a(\mu+i\omega)}{v_F}} \Gamma\left(0, -\frac{2a(\mu + i\omega)}{v_F}\right) + e^{\frac{2a(\mu+i\omega)}{v_F}} \Gamma\left(0, \frac{2a(\mu + i\omega)}{v_F}\right) \right\} + \frac{(\mu + i\omega)^2}{16\pi M {v_F}^5} \\ &\times \left\{ \frac{v_F[{v_F}^2 - 4a^2(\mu + i\omega)^2]}{2a^2(\mu + i\omega)^2} + e^{\frac{2a(\mu+i\omega)}{v_F}} [3v_F + 2a(\mu + i\omega)] \Gamma\left(0, \frac{2a(\mu + i\omega)}{v_F}\right) \right. \\ &\left. \times -e^{-\frac{2a(\mu+i\omega)}{v_F}} [-3v_F + 2a(\mu + i\omega)] \Gamma\left(0, -\frac{2a(\mu + i\omega)}{v_F}\right) \right\} + O\left(\frac{1}{M^2}\right) \end{aligned} \quad \text{(B6)}$$

and

$$\mathcal{I}_1^{(2)}(i\omega) = \frac{1}{8\pi {v_F}^2}\left\{\frac{{v_F}^2}{\mu+i\omega} - ae^{-\frac{2a(\mu+i\omega)}{v_F}}[-v_F+2a(\mu+i\omega)]\Gamma\left(0,-\frac{2a(\mu+i\omega)}{v_F}\right) - ae^{\frac{2a(\mu+i\omega)}{v_F}}[v_F+2a(\mu+i\omega)]\right.$$
$$\left.\times\,\Gamma\left(0,\frac{2a(\mu+i\omega)}{v_F}\right)\right\} + \frac{a(\mu+i\omega)}{8\pi M {v_F}^5}\left\{-2av_F(\mu+i\omega) + e^{\frac{2a(\mu+i\omega)}{v_F}}\left[2a^2(\mu+i\omega)^2+4av_F(\mu+i\omega)+{v_F}^2\right]\right.$$
$$\left.\times\,\Gamma\left(0,\frac{2a(\mu+i\omega)}{v_F}\right) - e^{-\frac{2a(\mu+i\omega)}{v_F}}\left[2a^2(\mu+i\omega)^2-4av_F(\mu+i\omega)+{v_F}^2\right]\Gamma\left(0,-\frac{2a(\mu+i\omega)}{v_F}\right)\right\} + O\left(\frac{1}{M^2}\right). \quad \text{(B7)}$$

For the second integral, we obtain

$$\mathcal{I}_2(i\omega_n,\mathbf{p}) = \frac{p}{8\pi v_F}\left\{\left[\left(\frac{1}{4M}\partial_a+\frac{v_F}{2}\right)\partial_a\partial_\mu - 1\right]\int_0^\infty dq\,\frac{e^{-2aq}}{\left(i\omega+\mu-\frac{q^2}{2M}+v_Fq\right)}\right\} = p\mathcal{I}_2^{(1)}(i\omega_n)+O(p^3), \quad \text{(B8)}$$

where

$$\mathcal{I}_2^{(1)}(i\omega) = -\frac{1}{4\pi {v_F}^2} + \frac{a(\mu+i\omega)}{4\pi {v_F}^3}\left\{e^{\frac{2a(\mu+i\omega)}{v_F}}\Gamma\left(0,\frac{2a(\mu+i\omega)}{v_F}\right) - e^{-\frac{2a(\mu+i\omega)}{v_F}}\Gamma\left(0,-\frac{2a(\mu+i\omega)}{v_F}\right)\right\}$$
$$-\frac{1}{8\pi M {v_F}^6}\left\{-2{v_F}^2(\mu+i\omega)+a(\mu+i\omega)^2\left[e^{-\frac{2a(\mu+i\omega)}{v_F}}[-3v_F+2a(\mu+i\omega)]\Gamma\left(0,-\frac{2a(\mu+i\omega)}{v_F}\right)+\right.\right.$$
$$\left.\left.\times\; e^{\frac{2a(\mu+i\omega)}{v_F}}[3v_F+2a(\mu+i\omega)]\Gamma\left(0,\frac{2a(\mu+i\omega)}{v_F}\right)\right]\right\} + O\left(\frac{1}{M^2}\right). \quad \text{(B9)}$$

Here, $\Gamma(0,z)$ is the Incomplete Gamma function, while $E_1(z)$ and $E_i(z)$ are the Exponential Integral functions.

The quasiparticle parameters introduced in Eqs. (13) and (14) in the main text are thus obtained from the expressions above, and they correspond to

$$\mathcal{I}_1^{(0)}(0) = \frac{1}{32\pi M v_F^5}\left\{\frac{v_F(v_F^2-4a^2\mu^2)}{a^2} + 2\mu e^{\frac{2a\mu}{v_F}}\left(\mu(2a\mu+3v_F)-2Mv_F^3\right)E_1\left(\frac{2a\mu}{v_F}\right) - 2\mu e^{-\frac{2a\mu}{v_F}}[\mu(2a\mu-3v_F)\right.$$
$$\left.+2Mv_F^3]\left[\mathrm{Ei}\left(\frac{2a\mu}{v_F}\right)+i\pi\right]\right\}, \quad \text{(B10)}$$

$$\frac{\partial\mathcal{I}_1^{(0)}}{\partial(i\omega)}(0) = -\frac{1}{8\pi M v_F^6}\left\{-e^{-\frac{2a\mu}{v_F}}\left[\mathrm{Ei}\left(\frac{2a\mu}{v_F}\right)+i\pi\right]\left(-2a^2\mu^3-2a\mu Mv_F^3+6a\mu^2v_F+Mv_F^4-3\mu v_F^2\right)\right.$$
$$\left.\times\,+e^{\frac{2a\mu}{v_F}}\left(-2a^2\mu^3+2a\mu Mv_F^3-6a\mu^2v_F+Mv_F^4-3\mu v_F^2\right)E_1\left(\frac{2a\mu}{v_F}\right)-2Mv_F^4+5\mu v_F^2\right\}, \quad \text{(B11)}$$

$$\mathcal{I}_1^{(2)}(0) = \frac{1}{8\pi M v_F^5}\left\{\frac{v_F(Mv_F^4-2a^2\mu^3)}{\mu} + ae^{\frac{2a\mu}{v_F}}\left[\mu\left(2a^2\mu^2+4a\mu v_F+v_F^2\right)-Mv_F^3(2a\mu+v_F)\right]E_1\left(\frac{2a\mu}{v_F}\right)\right.$$
$$\left.-\,ae^{-\frac{2a\mu}{v_F}}\left[\mu\left(2a^2\mu^2-4a\mu v_F+v_F^2\right)-Mv_F^3(v_F-2a\mu)\right]\left[\mathrm{Ei}\left(\frac{2a\mu}{v_F}\right)+i\pi\right]\right\}, \quad \text{(B12)}$$

$$\mathcal{I}_2^{(1)}(0) = \frac{1}{8\pi M v_F^7}\left\{-a\mu\left[e^{\frac{2a\mu}{v_F}}E_1\left(\frac{2a\mu}{v_F}\right)\left(\mu(2a\mu+3v_F)-2Mv_F^3\right)+e^{-\frac{2a\mu}{v_F}}\left[\mathrm{Ei}\left(\frac{2a\mu}{v_F}\right)+i\pi\right]\right.\right.$$
$$\left.\left.\times\,\left(\mu(2a\mu-3v_F)+2Mv_F^3\right)\right]-2v_F^2\left(Mv_F^2-\mu\right)\right\}. \quad \text{(B13)}$$

[1] S. Das Sarma, S. Adam, E. H. Hwang, and E. Rossi, Rev. Mod. Phys. **83**, 407 (2011).

[2] A. H. Castro Neto, F. Guinea, N. M. R. Peres, K. S. Novoselov, and A. K. Geim, Rev. Mod. Phys. **81**, 109 (2009).

[3] N. M. R. Peres, Rev. Mod. Phys. **82**, 2673 (2010).

[4] E. Muñoz, J. Phys.: Condens. Matter **24**, 195302 (2012).

[5] E. Muñoz, J. Lu, and B. I. Yakobson, Nano Lett. **10**, 1652 (2010).

[6] N. An, T. Tan, Z. Peng, C. Qin, Z. Yuan, L. Bi, C. Liao, Y. Wang, Y. Rao, G. Soavi, and B. Yao, Nano Lett. **20**, 6473 (2020).

[7] A. Azizi, M. Dogan, H. Long, J. D. Cain, K. Lee, R. Eskandari, A. Varieschi, E. C. Glazer, M. L. Cohen, and A. Zettl, Nano Lett. **20**, 6120 (2020).

[8] Z. Gao, H. Xia, J. Zauberman, M. Tomaiuolo, J. Ping, Q. Zhang, P. Ducos, H. Ye, S. Wang, X. Yang, F. Lubna, Z. Luo, L. Ren, and A. T. C. Johnson, Nano Lett. **18**, 3509 (2018).

[9] F. Yavari and N. Koratkar, J. Phys. Chem. Lett. **3**, 1746 (2012).

[10] Z. Zhang, X. Zhang, W. Luo, H. Yang, Y. He, Y. Liu, X. Zhang, and G. Peng, Nanoscale Res. Lett **10**, 359 (2015).

[11] Y.-H. Zhang, Y.-B. Chen, K.-G. Zhou, C.-H. Liu, J. Zeng, H.-L. Zhang, and Y. Peng, Nanotechnology **20**, 185504 (2009).
[12] S. Chen, W. Cai, D. Chen, Y. Ren, X. Li, Y. Zhu, J. Kang, and R. S. Ruoff, New J. Phys. **12**, 125011 (2010).
[13] W. H. Appelt, A. Droghetti, L. Chioncel, M. M. Radonjić, E. Muñoz, S. Kirchner, D. Vollhardt, and I. Rungger, Nanoscale **10**, 17738 (2018).
[14] M. A. H. Vozmediano, M. I. Katsnelson, and F. Guinea, Phys. Rep. **496**, 109 (2010).
[15] F. de Juan, M. Sturla, and M. A. H. Vozmediano, Phys. Rev. Lett. **108**, 227205 (2012).
[16] E. Arias, A. R. Hernández, and C. Lewenkopf, Phys. Rev. B **92**, 245110 (2015).
[17] H. Falomir, M. Loewe, E. Muñoz, and A. Raya, Phys. Rev. B **98**, 195430 (2018).
[18] M. Zarenia, A. Chaves, G. A. Farias, and F. M. Peeters, Phys. Rev. B **84**, 245403 (2011).
[19] H. Falomir, E. Muñoz, M. Loewe, and R. Zamora, J. Phys. A **53**, 015401 (2020).
[20] H. Falomir, J. Gamboa, M. Loewe, and M. Nieto, J. Phys. A **45**, 135308 (2012).
[21] J. Rammer and H. Smith, Rev. Mod. Phys. **58**, 323 (1986).
[22] A. Hewson, J. Phys.: Condens. Matter **13**, 10011 (2001).
[23] V. Pandis and A. C. Hewson, Phys. Rev. Lett. **115**, 076401 (2015).
[24] E. Muñoz, C. J. Bolech, and S. Kirchner, Phys. Rev. Lett. **110**, 016601 (2013).
[25] M. S. Foster and I. L. Aleiner, Phys. Rev. B **77**, 195413 (2008).
[26] N. Menezes, V. S. Alves, E. C. Marino, L. Nascimento, L. O. Nascimento, and C. Morais Smith, Phys. Rev. B **95**, 245138 (2017).
[27] M. Beneke and M. Jamin, J. High Energy Phys. 09 (2008) 044.
[28] P. Fendley, Phys. Lett. B **196**, 175 (1987).
[29] D. K. Efetov and P. Kim, Phys. Rev. Lett. **105**, 256805 (2010).